

Natural Silica Sand/Alumina Ceramic Composites: Promising Candidates for Fuel-Cell Sealants

N Hidayat¹, Istiqomah², M Y H Widiyanto³, A Taufiq^{1,4}, Sunaryono^{1,4}, Triwikantoro³, M Zainuri³, M A Baqiya³, G Aristia⁵ and S Pratapa³

¹Department of Physics, Faculty of Mathematics and Natural Sciences, Universitas Negeri Malang (State University of Malang), Jl. Semarang 5, Malang 65145, Indonesia

²National Standardization Agency of Indonesia, Jl. M. H. Thamrin No 8, Kebon Sirih, Jakarta Pusat 10340, Indonesia

³Department of Physics, Faculty of Mathematics and Natural Sciences, Institute of Technology Sepuluh Nopember, Jl. Arif Rachman Hakim, Surabaya 60111, Indonesia

⁴Center for Minerals and Advanced Materials, Faculty of Mathematics and Natural Sciences, Universitas Negeri Malang (State University of Malang), Jl. Semarang 5, Malang 65145, Indonesia

⁵Department of Physical and Theoretical Chemistry, Institute of Chemistry and Biochemistry, Freie Universität Berlin, Kaiserswerther Str. 16-18, 14195, Germany

Email: nurul.hidayat.fmipa@um.ac.id

Abstract. An attempt has been developed to establish the prospect of the useful application of Indonesian natural silica sand, instead of commercially expensive materials, as a future fuel-cell sealant. The sand was initially washed and ball-milled at 150 rpm for 60 minutes and then heated at 1000 °C for the same duration. The resulting powder was then mixed with alumina powder at various amounts and shaped into discs before sintering at 1150 °C and 1250 °C to produce compact ceramics. The diameter shrinkage, porosity, and density of the ceramics were evaluated by Archimedes method. Their crystalline phase composition was quantified by Rietveld refinement analysis on the X-ray diffraction (XRD) data and the phase weight fraction was then used for coefficient of thermal expansion (CTE) evaluation. It was observed that the bulk density increased while the porosity decreased with alumina addition. The XRD data analysis revealed that the prepared silica sand contains a very high purity of quartz-SiO₂, i.e. 97.8(18)%. The sintering temperatures of 1150 °C and 1250 °C transformed some quartz-SiO₂ to cristobalite-SiO₂. All the calcite-CaCO₃ exhibited reaction sintering with SiO₂ forming wollastonite-CaSiO₃. Therefore, the ceramic composites contained SiO₂/Al₂O₃/CaSiO₃. Regarding CTE, all of the composites meet the criteria for fuel-cell sealants, in the range of 9-12 ppm/°C.

Keywords: Indonesian silica sand, alumina, phase quantification, coefficient of thermal expansion, fuel-cell sealant.



1. Introduction

In light of finding future clean energy technologies, solid oxide fuel cells (SOFCs) are recognized as one of the most environmentally friendly and feasible energy conversion devices [1,2]. It is due to their very long life expectancy [3], high efficiency [4], and fuel flexibility properties [5]. The SOFCs, devices that convert the chemical energy of fuels into electricity, have been extensively studied to reduce CO₂ emission and fossil fuel consumption [6]. In spite of this, it is confronted with a challengeable task on preventing leakage when an SOFC operates at high temperature (800-1000 °C) [7]. Consequently, a proper gas-tight sealing material plays a decisive role to obtain the best operation and performance of SOFCs [8]. The very basic criteria for fuel cell sealing material are the CTE, which must be in the range of 9-12 ppm/°C [9], and thermo-mechanically and chemically stable [10]. The matching of CTE of the fuel-cell sealing materials to other cell components is essential to minimize the thermal stresses [11].

Recently, ceramic-based composites and glass-ceramics have become highly recommended sealing materials for various SOFCs attributable to their superior characteristics compared with those of metallic sealants, mainly to resist both reducing and oxidizing environments [12,13]. Additionally, they also perform excellent gas tightness and provide CTE similar to those of the other stack components [14]. Numerous investigations have been conducted in search of great fuel cell sealants, e.g. 30CaO–40SiO₂–20B₂O₃–10A₂O₃ (A = Y, La) [7], Al₂O₃–glass composite [13], and (1–x)[SrO–SiO₂–B₂O₃]_{1–x}Al₂O₃ [15]. Al₂O₃/SiO₂-based sealants show an excellent performance in maximizing the SOFC operation [16]. However, rarely has a research exclusively explored the use of natural silica-based materials as the SiO₂ source for fuel cell sealants production.

In this present study, we introduce the prospect of using Indonesian silica sand as the fuel cell sealing material. This breakthrough is crucial not only to minimize the fabrication cost of alumina/silica-based fuel cell sealants but also to elevate the added-value of the abundant natural silica sand resources. As one of the most abundant naturally-occurring materials, SiO₂ can be predominantly found in silica sand [17]. Indonesia becomes a country that serves a significant amount of natural silica sand. It can be revealed from the facts that (1) Indonesia is the largest archipelagic nation with roughly 67% sea and (2) it is one of the world's top five countries with the longest coastlines imply many advantages regarding its mineral resources [18]. Also, our previous preliminary studies [19,20] reported that Indonesian silica sand from coastal district of Tuban comprised of very high quartz-SiO₂ content. The results lead to a must-solved research question of establishing the potential of natural silica sand/alumina ceramic composites for fuel-cell sealants that is described in this paper.

2. Experimental Methods

High purity quartz-SiO₂ was extracted from natural silica sand from Indonesian Beach, particularly located in Tuban area. The selected sands were simply washed by using water and dried overnight. The dried silica sands were then mechanically sieved to obtain fine powders and magnetically extracted to eliminate the magnetic constituents. The typical silica sands were ball-milled at 150 rpm for 60 minutes followed by sintering at 1000 °C for other 60 minutes. The elemental contents of the prepared SiO₂ were reported elsewhere [19,20]. Alumina (PA, Sigma-Aldrich) with various concentrations were ground with the prepared silica before 4-hour sintering at 1150 °C and 1250 °C.

The prepared powder was then uniaxially pressed with a force of 600 N to produce a cylindrical-shaped sample with a diameter of 1.3(1) cm for density-porosity measurement. X-ray diffraction (XRD) using Cu-K α radiation was applied to evaluate the phase profiling in the sample. Density-porosity was measured by means of Archimedes method following the Australian standard of 1774.5. Rietveld refinement approach was executed to analyze the relative weight fractions of each phase [21] via Rietica software [22] as the crystalline phase identification was completely accomplished by means of X'Pert High Score Plus software [23]. The relative weight fractions were then converted to volume fraction for CTE composite evaluations. Additionally, the nomenclatures for sample identifications were given by using the following naming convention. "NSS" refers to natural silica sand, "A" refers to alumina, and "1150" (or "1250") relates to the sintering temperature. Therefore, "NSS1A" means a composite of

natural silica sand with the addition of 10% alumina. “NSS3A1250” means a composite of natural silica sand with 30% of alumina addition and 1250 °C sintering temperature.

3. Results and Discussion

The physical data for all composites in terms of diameter shrinkage, porosity, and bulk density (*note*: a terminology of “density” in this paper always refers to “bulk density” unless there is another detail) are depicted in Table 1. Based on Table 1, it can be seen that the highest diameter shrinkage is -0.19(1) mm for NSS1250. Such shrinkage is believed due to the external pressure and sintering treatment [24]. Other factors that affect shrinkage are inhomogeneous particle shape [25] and porous shape [26].

In general, an addition of Al₂O₃ increases the composite’s density and reduces its porosity. At a sintering temperature of 1250 °C, the porosity of NSS1250 decreases 1.22% from the porosity of NSS1150. The porosities of NSS1A1250, NSS2A1250, and NSS3A1250 are, respectively, 29.61(4)%, 29.07(4)%, and 28.98(4)%. The highest density was obtained when the sample has 30% Al₂O₃ content for both sintering temperatures. The addition of 30% Al₂O₃ to the SiO₂ increases the density of as much as 0.19 g/cm³ and 0.31 g/cm³, respectively at 1150 °C and 1250 °C sintering temperatures. Additionally, those increments of the composites density result from the presence of crystalline phases formed in the samples.

Phase identification and quantification are necessary to evaluate the coefficient of thermal expansion (CTE) of the composites. The results are also essential to justify chemical reactions between silica and alumina. The XRD profiles of the composites after sintering are depicted in Figure 1. The phase compositions of natural silica sand/alumina composites are given in Table 3. The phase identification verifies that all the XRD profiles contain quartz-SiO₂ (PDF reference code: 00-046-1045), corundum-Al₂O₃ (01-075-1862), wollastonite-CaSiO₃ (01-075-1396), and cristobalite-SiO₂ (01-077-1317). An example of the phase identification analysis result (sample NSS1A1150) is listed in Table 2. Full pattern Rietveld refinement gives more precise phase quantification data for the representative samples as depicted in Table 3.

Table 3 tells that calcite does not further exist. Wollastonite occurred as a consequence of reaction between SiO₂ and CaO during the sintering process. CaO could come from CaCO₃ decomposition within the natural silica sand at a temperature of, at least, 895 °C [27]. CaCO₃ was detected in the as prepared silica sand. The processed silica sand, based on Rietveld refinement on XRD data, contained quartz-SiO₂ and calcite-CaCO₃ with weight fractions of 97.8(18)% and 2.2(2)%, respectively (the XRD data is not shown). The contribution of calcium oxide in wollastonite formation is not merely influenced by CaO, or CaCO₃ decomposition. It also comes from the alumina itself (from XRF data of alumina, it contains 1.1(1)% calcium), though the contribution is subtle. The wollastonite formation is given in Equation 1 [28,29]:



Table 1. Physical properties of natural silica sand/alumina ceramic composites (the values in parentheses are the estimated standard deviation to the left).

Sample	Δd (mm)	P (%)	ρ (g/cm ³)
NSS1150	-0.09(1)	36.37(9)	2.65(1)
NSS1A1150	-0.09(1)	30.21(4)	2.64(1)
NSS2A1150	-0.07(1)	29.94(4)	2.71(1)
NSS3A1150	-0.07(1)	29.80(4)	2.84(1)
NSS1250	-0.19(1)	35.15(9)	2.46(1)
NSS1A1250	-0.05(1)	29.61(4)	2.57(1)
NSS2A1250	-0.03(1)	29.07(4)	2.62(1)
NSS3A1250	-0.02(1)	28.98(4)	2.77(1)

Note: Δd = diameter shrinkage, P = porosity, and ρ = density.

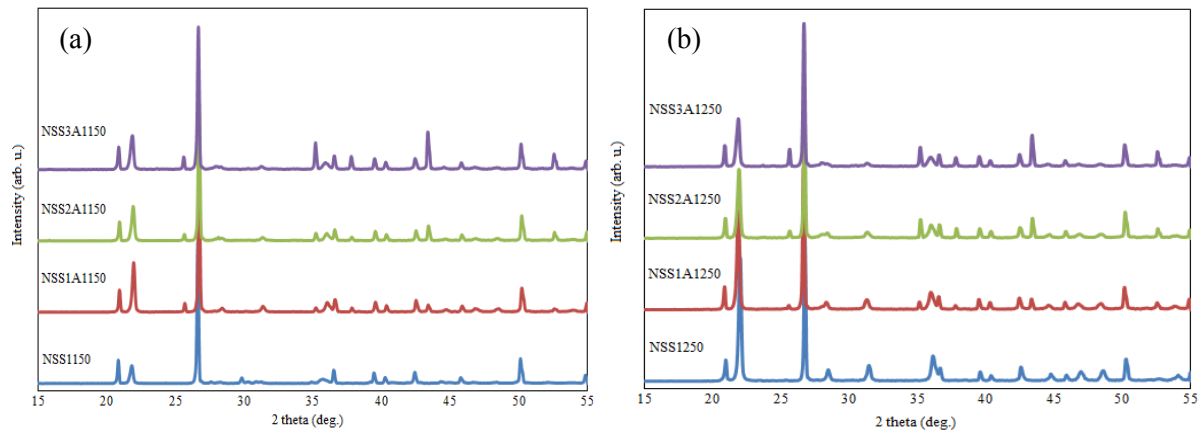


Figure 1. XRD profiles (Cu-K α radiation) of the processed silica sand and the composites; (a) after sintered at 1150 °C and (b) after sintered at 1250 °C.

Table 2. Phase identification of NSS1A1150 by means of X'Pert High Score Plus.

Position (2 θ deg.)	Relative Intensity (%)	Identified Crystalline Phase
20.96	15.10	Quartz-SiO ₂
21.99	32.68	Cristobalite-SiO ₂
25.71	6.25	Corundum-Al ₂ O ₃
26.75	100.00	Quartz-SiO ₂
28.43	2.46	Cristobalite-SiO ₂
31.40	3.36	Wollastonite-CaSiO ₃
35.24	2.94	Corundum-Al ₂ O ₃
36.06	6.14	Cristobalite-SiO ₂
36.66	7.92	Quartz-SiO ₂
37.88	2.44	Quartz-SiO ₂
39.58	6.80	Quartz-SiO ₂
40.40	3.93	Quartz-SiO ₂
42.53	7.99	Quartz-SiO ₂
43.41	4.83	Corundum-Al ₂ O ₃
44.73	1.39	Cristobalite-SiO ₂
45.88	4.03	Quartz-SiO ₂
46.88	1.99	Cristobalite-SiO ₂
48.60	1.61	Cristobalite-SiO ₂
50.22	17.52	Quartz-SiO ₂
52.58	2.16	Corundum-Al ₂ O ₃
54.02	1.11	Cristobalite-SiO ₂

Meanwhile, the cristobalite within the samples is caused by phase transformation of the quartz-SiO₂ due to thermal treatment since quartz transformed to be cristobalite at a temperature above 1000 °C [30]. Such fact is in line with the result found in this experiment; cristobalite occurred at the temperature of 1150 °C. The addition of Al₂O₃ decreases the concentration of SiO₂. Therefore, the reduction of cristobalite as the addition of Al₂O₃ undoubtedly happens.

Table 3. Rietveld relative weight fraction of crystalline phases in natural silica sand/alumina ceramic composites (the values in parentheses are the estimated standard deviation).

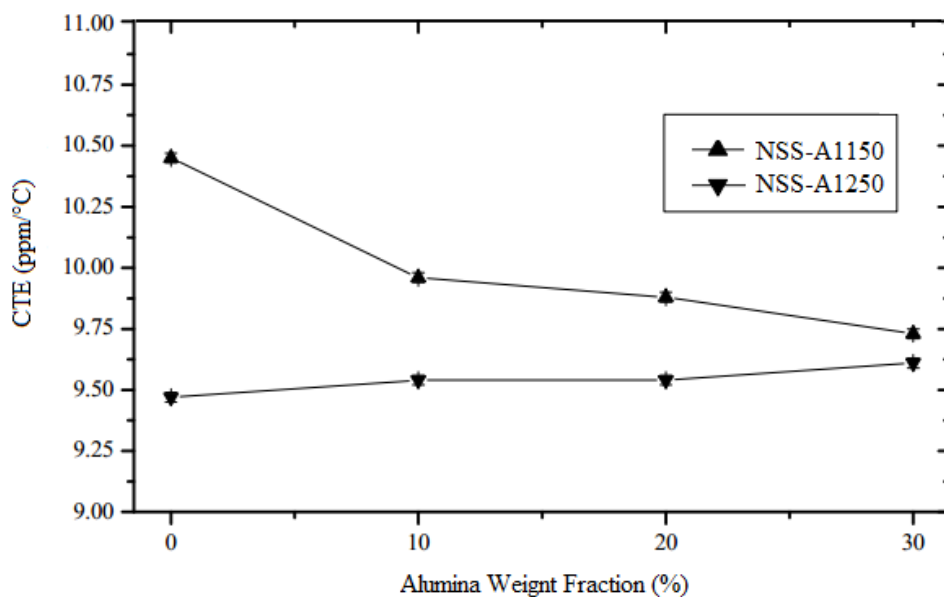
Sample	Relative Weight Fraction (%)			
	Quartz (SiO ₂)	Corundum (Al ₂ O ₃)	Wollastonite (CaSiO ₃)	Cristobalite (SiO ₂)
NSS1150	61.3(19)	-	7.0(7)	31.7(10)
NSS1A1150	55.4(21)	10.4(28)	1.8(1)	33.2(27)
NSS2A1150	49.7(13)	19.1(15)	1.4(3)	29.8(10)
NSS3A1150	41.4(20)	30.2(17)	1.3(1)	27.1(38)
NSS1250	26.5(19)	-	6.1(8)	67.4(22)
NSS1A1250	40.3(16)	10.2(8)	1.0(2)	48.6(31)
NSS2A1250	37.8(10)	20.4(10)	0.9(2)	40.8(13)
NSS3A1250	37.6(18)	30.6(34)	1.0(2)	30.8(19)

Once SiO₂-Al₂O₃ phase diagram is taken into consideration to explain the phenomena observed in this experimental results, a question should arise as follows “why does not mullite, 3Al₂O₃·2SiO₂ exist?”. According to the SiO₂-Al₂O₃ phase diagram [31], the solidus of mullite shifts as the alumina increases above the eutectic point. Nucleation and growth of mullite start to occur above the sintering temperature of 1587 °C [31] since quartz completely transforms to cristobalite at 1570 °C [30]. Hence, it makes sense that mullite was not observed by XRD yet.

An understanding of the composite performance, based on the constituent materials, is important not only for practical purposes like predicting the composite properties, e.g. CTE but also as fundamental knowledge to develop new materials [32]. After converting the weight fractions in Table 3 to volume fractions, CTE values prediction can be made by applying Halpin-Tsai equation [33,34] as given in Equation 2. The CTE characteristics of the samples are shown in Figure 3.

$$\alpha_c = \alpha_m \frac{1 + 2sqV_f}{1 - qV_f} \quad (2)$$

Where $q = (\alpha_r - 1) / (\alpha_r + 2s)$ and $\alpha_r = \alpha_f / \alpha_m$, α represents CTE, V represents volume, and s represents the dimensional ratio between reinforcement and matrix; for isotropic composite, $s = 1$. Subscripts c, f , and m , respectively refer to composite, filler, and matrix.

**Figure 2.** CTE prediction values for SiO₂/Al₂O₃/CaSiO₃ after XRD phase compositional Rietveld analysis.

As noticeably pictured in Figure 2, an addition of Al_2O_3 for the sintering temperature of 1150°C reduces the CTE of the composites. It is because of the smaller CTE of corundum compared with quartz as the predominant phase in the composites. This finding is in good agreement with another literature [35]. Moreover, at the same time, an addition of Al_2O_3 for the sintering temperature of 1250°C conversely elevates the CTE of the composites. It is because of the increasing amount of cristobalite (see Table 3) and volume fraction of corundum which is no longer able to decrease the CTE of the composites. On top of that, all $\text{SiO}_2/\text{Al}_2\text{O}_3/\text{CaSiO}_3$ composites show excellent CTE matching to those of fuel-cell components, with CTE values in the range of $9\text{--}12\text{ ppm}/^\circ\text{C}$.

4. Conclusion

This present study concludes that the natural silica sand from Tuban area is a promising candidate as a fuel cell sealing material with the incorporation of alumina. The 4-hour sintering at temperatures of 1150°C and 1250°C has transformed some quartz- SiO_2 to cristobalite- SiO_2 . Calcite- CaCO_3 within the samples completely reacted with SiO_2 forming wollastonite- CaSiO_3 . Thus, the ceramic composites encompassed $\text{SiO}_2/\text{Al}_2\text{O}_3/\text{CaSiO}_3$. Finally, regarding CTE, all of the composites meet the criteria for fuel cell sealants.

5. References

- [1] Sabato A G *et al* 2016 Glass-ceramic sealant for solid oxide fuel cells application: Characterization and performance in dual atmosphere *J. Power Sources* **328** 262–270
- [2] Sharifzadeh M, Meghdari M and Rashtchian D 2017 Multi-objective design and operation of solid oxide fuel cell (SOFC) triple combined-cycle power generation systems: Integrating energy efficiency and operational safety *Appl. Energy* **185**(1) 345–361
- [3] Choudhury A, Chandra H and Arora A Application of solid oxide fuel cell technology for power generation-A review *Renew. Sustain. Energy Rev.* **20** 430–442
- [4] Irvine J T S, Neagu D, Verbraeken M C, Chatzichristodoulou C, Graves C and Mogensen M B 2016 Evolution of the electrochemical interface in high-temperature fuel cells and electrolyzers *Nat. Energy* **1** 15014
- [5] Yang L *et al* 2009 Enhanced sulfur and coking tolerance of a mixed ion conductor for SOFCs: $\text{BaZr}_{0.1}\text{Ce}_{0.7}\text{Y}_{0.2-x}\text{Yb}_x\text{O}_{3-\delta}$ *Science* **326**(5949) 126–129
- [6] Sandhu N K *et al* 2016 Electrochemical performance of a short tubular solid oxide fuel cell stack at intermediate temperatures *Appl. Energy* **183** 358–368
- [7] Kumar V, Rupali, Pandey O P and Singh K Thermal and crystallization kinetics of yttrium and lanthanum calcium silicate glass sealants for solid oxide fuel cells *Int. J. Hydrog. Energy* **36**(22) 14971–76
- [8] Reddy A A *et al* 2013 Diopside–Ba disilicate glass–ceramic sealants for SOFCs: Enhanced adhesion and thermal stability by Sr for Ca substitution *Int. J. Hydrog. Energy* **38**(7) 3073–86
- [9] Mahapatra M K and Lu K 2010 Seal glass for solid oxide fuel cells *J. Power Sources* **195**(21) 7129–39
- [10] Malzbender J, Wakui T and Steinbrech R W 2006 Curvature of planar solid oxide fuel cells during sealing and cooling of stacks *Fuel Cells* **6**(2) 123–129
- [11] Ghosh S, Kundu P, Sharma A D, Basu R N and Maiti H S 2008 Microstructure and property evaluation of barium aluminosilicate glass–ceramic sealant for anode-supported solid oxide fuel cell *J. Eur. Ceram. Soc.* **28**(1) 69–76
- [12] Bause T, Malzbender J, Pausch M, Beck T and Singheiser L 2013 Damage and failure of silver based ceramic/metal joints for SOFC stacks *Fuel Cells* **13**(4) 578–583
- [13] Zhang W *et al* 2016 Development of flexible ceramic-glass seals for intermediate temperature planar solid oxide fuel cell *Int. J. Hydrog. Energy* **41**(14) 6036–44
- [14] Nguyen X V *et al* 2016 Study of sealants for SOFC *Int. J. Hydrog. Energy* **41**(46) 21812–19

- [15] Kim E A, Choi H W and Yang Y S 2015 Effects of Al_2O_3 on $(1-x)[\text{SrO}-\text{SiO}_2-\text{B}_2\text{O}_3]-x\text{Al}_2\text{O}_3$ glass sealant for intermediate temperature solid oxide fuel cell *Ceram. Int.* **41**(10) Part B 14621–26
- [16] Dai Z, Pu J, Yan D, Chi B and Jian L 2011 Thermal cycle stability of Al_2O_3 -based compressive seals for planar intermediate temperature solid oxide fuel cells *Int. J. Hydrog. Energy* **36**(4) 3131–37
- [17] Nesse W 2011 *Introduction to Mineralogy* 2nd edition (New York: Oxford University Press)
- [18] Brotosusilo A, Apriana I W A, Satria A A and Jokopitoyo T 2016 Littoral and coastal management in supporting maritime security for realizing indonesia as world maritime axis *IOP Conf. Ser. Earth Environ. Sci.*, **30**(1) 012016
- [19] Aristia G A G, Istiqomah, Hidayat N, Triwikantoro, Baqiya M A and Pratapa S 2015 Phase analysis of natural silica-sand-based composites as potential fuel-cell seal material *Adv. Mater. Res.* **1112** 294–298
- [20] Hidayat N, Triwikantoro, Baqiya M A and Pratapa S 2013 Thermal expansion coefficient prediction of fuel-cell seal materials from silica sand *AIP Conf. Proc.* **1555** 99–101
- [21] Rietveld H M 1969 A profile refinement method for nuclear and magnetic structures *J. Appl. Crystallogr.* **2**(2) 65–71
- [22] Hunter B A 1998 Rietica-A visual Rietveld program *Newsl. Int. Union Crystallogr. Comm. Powder Diffraction*
- [23] Degen T, Sadki M, Bron E, König U and Nénert G 2014 The HighScore suite *Powder Diffraction* **29**(S2) S13–S18
- [24] Olevsky E and Skorohod V 1993 Deformation aspects of anisotropic-porous bodies sintering *J. Phys. IV* **03**(C7) 739–742
- [25] Zavaliangos A, Missiaen J M and Bouvard D 2006 Anisotropy in shrinkage during sintering *Sci. Sinter.* **38**(1) 13–25
- [26] Ch'ng H N and Pan J 2007 Sintering of particles of different sizes *Acta Mater.* **55**(3) 813–824
- [27] L'vov B V, L'vov B V, Polzik L K and Ugolkov V L 2002 Decomposition kinetics of calcite: a new approach to the old problem *Thermochim. Acta* **390**(1–2) 5–19
- [28] Deer W A, Howie R A and Zussman J 1997 *Single-Chain Silicates* Geological Society
- [29] Tavangarian F and Emadi R 2010 Synthesis of nanocrystalline forsterite (Mg_2SiO_4) powder by combined mechanical activation and thermal treatment *Mater. Res. Bull.* **45**(4) 388–391
- [30] Day A L and Shepherd E S 1906 The lime-silica series of minerals *J. Am. Chem. Soc.* **28**(9) 1089–114
- [31] Tse J S and Klug D D 1991 The structure and dynamics of silica polymorphs using a two-body effective potential model *J. Chem. Phys.* **95**(12) 9176–85
- [32] Karadeniz Z H and Kumlutas D 2007 A numerical study on the coefficients of thermal expansion of fiber reinforced composite materials *Compos. Struct.* **78**(1) 1–10
- [33] Affdl J C H and Kardos J L 1976 The Halpin-Tsai equations: A review *Polym. Eng. Sci.* **16**(5) 344–352
- [34] Pascual M J, Guillet A and Durán A 2007 Optimization of glass–ceramic sealant compositions in the system $\text{MgO}-\text{BaO}-\text{SiO}_2$ for solid oxide fuel cells (SOFC) *J. Power Sources* **169**(1) 40–46
- [35] Wang X *et al* 2013 Optimization of Al_2O_3 –glass composite seals for planar intermediate-temperature solid oxide fuel cells *J. Power Sources* **226** 127–133